Rheol Acta (2008) 47:435–446
DOI 10.1007/s00397-008-0263-6

ORIGINAL CONTRIBUTION

Localised flow-induced crystallisation of a polyethylene melt

D. G. Hassell · M. R. Mackley

Received: 15 June 2007 / Revised: 8 January 2008 / Accepted: 22 January 2008 / Published online: 27 February 2008

Abstract The sensitivity of flow-induced crystallisation (FIC) to the nature of flow type is demonstrated using a high-density polyethylene (HDPE) for two different flow geometries. A contraction–expansion slit geometry was used to create a mixed, but primarily simple shear flow, while a cross-slot geometry provided a region within the flow of high extension. Flow-induced birefringence was captured at a melt processing temperature of 155 °C to identify the principal stress difference within the two flows and determine regions of higher stress within the HDPE. The experiments were then repeated at 125 °C, and FIC was identified using bright-field observation. Crystallisation was observed within the regions that previously exhibited high stress levels. It was found that lower deformation rates in pure shear were required when compared with simple shear to create the crystal filaments.

Keywords Flow-induced crystallisation · Crystallisation · Flow visualisation · Birefringence

Introduction

In polymer processing, flow, molecular orientation and molecular stretch affect the crystallisation process and influence the orientation, morphology and mechanical properties of the final solid product. In the absence of flow, polymers crystallise to form spherulitic superstructures (see for example Keller 1968). Initial studies of flow-induced crystallisation (FIC) of polymers found that both extensional (van-der Vegt and Smit 1967) and shear flow (Haas and Maxwell 1969) can induce crystallisation above the quiescent crystallisation temperature range. Early work focussed mainly on polymer solutions and culminated in the discovery of the shish-kebab morphology (Pennings and Kiel 1965; Keller 1968), which were observed in both stirred vessels (Pennings and Kiel 1965) and a rotating cylinder device (Iguchi et al. 1966). In the latter case, the onset of shish-kebab crystallisation was related to the rotational speed at which Taylor vortices started to form, and fibres were generated within the elongational region at the centre of the vortices (Pennings and Kiel 1965; Mackley 1972).

More recently, there have been extensive studies of FIC from a number of research groups throughout the world (see for example Doufas et al. 1999; Guo et al. 1999; Jay et al. 1999; Nogales et al. 2001; Zuidema et al. 2001; Janeschitz-Kriegl et al. 2003; van Meerveld et al. 2004; Heeley et al. 2006; Acierno et al. 2003; Byelov et al. 2007; Hadinata et al. 2007; Kimata et al. 2007). Hadinata et al. (2007) investigated FIC of the same material using both parallel plate simple shear and uniaxial extensional flow, applying viscosity as a measure of crystallisation. The extensional flow displayed a greater enhancement on crystallisation kinetics because of the greater molecular orientation produced by this type of flow for similar deformation rates.

For more complex flows, numerous bright-field observations have been performed in a long slit die. This flow exhibits predominantly shear flow, with high levels of shear at the walls, and it was within these regions of the flow that crystallisation was observed (Mackley et al. 2000; Hadinata et al. 2006; Scelsi, private communication; Hernandez de Muller 2007). Various devices have been used to investi-

D. G. Hassell · M. R. Mackley (✉)
Department of Chemical Engineering, University of Cambridge,
Pembroke Street,
Cambridge CB2 3RA, UK
e-mail: mrm5@cheng.cam.ac.uk

gate extensional flow, and these include impinging jets (Mackley 1972), a four-roll mill (Crowley et al. 1976) and a cross-slot device (Swartjes 2001). Both bright-field observation and optical birefringence found crystallisation within the extensional regions of the flow emanating from the stagnation point at the centre of the flow.

Modelling of FIC is difficult and, in most cases, is limited to using the Avrami model of nucleation and growth (Avrami 1939) as a frame of reference (see for instance, more recent work by Doufas et al. 1999; Smirnova et al. 2005). A recent review (van Meerveld et al. 2004) concluded that molecular orientation and stretch were important for enhanced crystallisation, while the high molecular weight (HMW) chains govern the FIC dynamics. This HMW sensitivity has been observed in other work (Jay et al. 1999; Nogales et al. 2001; Heeley et al. 2006; Hadinata et al. 2007; Kimata et al. 2007). Other work (Janeschitz-Kriegl 2003; Janeschitz-Kriegl et al. 2003) has suggested the application of a critical work criteria to describe the onset of FIB, successfully applied to enhanced shear-induced isothermal crystallisation in isotactic polypropylene (Chen et al. 2006). These studies illustrate an increasing understanding of the physics taking place during the complex process of FIC.

Recent advances in constitutive models and computational techniques now mean that is it possible to accurately predict the behaviour of molten polymers flowing through complex geometries (see for example Peters et al. 1999; Lee et al. 2001; Agassant et al. 2002; Bent et al. 2003; Valette et al. 2006). The application of FIC kinetics to these techniques is currently being developed to allow the prediction of FIC in these complex flows (see for example Zuidema et al. 2001 and Smirnova et al. 2005). However, before an accurate comparison between prediction and experimentation is possible, controlled experimental results for both flow types are required, which use a polymer of known architecture under tightly controlled flow conditions. In this paper, an experimental comparison is presented of the effect of predominantly simple shear and extensional flow on FIC for the same polymer and temperature. A polydisperse polyethylene, the subject of successful ab initio linear rheological characterisation from molecular theory (Das et al. 2006), was used in both geometries under the same thermal conditions. The regions of high stress within the flow were identified using flow-induced birefringence at a temperature ~30 °C above the quiescent melting point. Subsequently, bright-field studies were then performed at a temperature slightly above the quiescent crystallisation temperature where FIC only was observed. This work provides a robust test for predictive FIC models under different flow conditions while simultaneously providing insight into some of the physical mechanisms through which FIC occurs.

Materials and methods

Materials

The material used was a polydisperse high-density polyethylene (HDPE), labelled HDB6. It has a M_w of 68,000 g/mol, M_w/M_n of 2.08 and comes from a family of HDPE materials having increasing levels of long-chain branching. Differential scanning calorimetry identified the following quiescent crystallisation temperatures; crystallisation onset ~123 °C, peak ~120 °C and end ~113 °C. Unlike many commercial polyethylenes, HDB6 has a predictable architecture and has been used in recent experimental (Wood-Adams and Costeux 2001) and theoretical (Das et al. 2006) studies where the ab initio theoretical modelling successfully captured the linear rheological response of the material.

Experimental processing geometries

A Cambridge multi-pass rheometer (MPR; Mackley et al. 1995) was used for the processing experiments, and its application with an optical configuration has been previously described by a number of authors (see for instance Collis and Mackley 2005). The MPR is a dual-piston capillary-type rheometer designed for small quantities of material (~10 g of polymer) and consists of three sections. The top and bottom sections contain reservoirs for the polymer material, servo hydraulically driven pistons and pressure/temperature transducers. The midsection enables simultaneous pressure and optical measurements to be made and resembles a cube with holes in all six faces. The vertical faces accept a pair of stainless steel die inserts in one direction and a pair of stress-free quartz windows in the other, while polymer flows through the top and bottom holes. All three sections are surrounded by heating channels and insulation.

Two different geometries were investigated. The first was a contraction–expansion (CE) slit geometry similar to those used in previous work (see for instance Collis and Mackley 2005). This geometry creates regions of high simple shear near to the slit walls and extensional flow in the region of the symmetry line in the inlet and outlet areas of the flow. The second is a cross-slot geometry. This flow configuration creates a pure shear flow deformation in the central region about the stagnation point of the flow, together with essentially simple shear near the outer curved walls (see for instance Coventry and Mackley 2008).

The two insert geometries used during this study are shown in Fig. 1. For the CE slit inserts, the material can be repeatedly passed through the midsection, from one reservoir to the other and back again at different flow rates, allowing multiple experiments to be performed on one

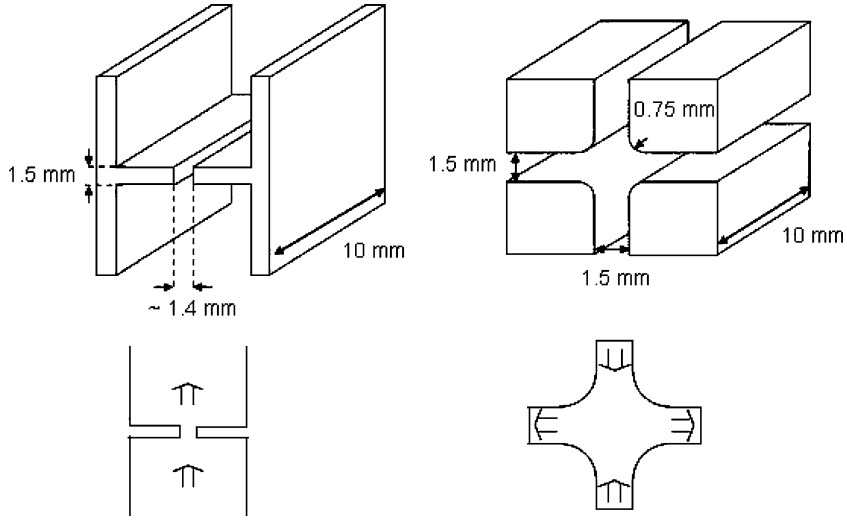

Fig. 1 The geometries used in the MPR midsection and associated flow directions for (*left*) contraction–expansion slot and (*right*) the cross-slot

sample. Optical observation of the CE slit section enabled interrogation of the entry and exit flow together with flow within the slit. The inserts used for the cross-slot geometry utilised slave pistons, which used a pressurised nitrogen system to facilitate multi-pass operation. The system was developed by Coventry (2006) and is reported by Coventry and Mackley (2008). During operation, the two MPR pistons are moved towards one another at a controlled rate, pushing material through the top and bottom of the insert and out through two horizontal side channels. Slave pistons in these horizontal channels maintain the material within the MPR, and the subsequent retraction of the pistons to their original position allows the pressurised nitrogen to force the material back through the cross-slot and into the top and bottom reservoirs. A schematic illustration of the MPR for both geometries is shown in Fig. 2.

Both geometries have been used in previous work (Coventry and Mackley 2008; Hassell et al. 2008) and are 10-mm deep. While the cross-slot and contraction–expansion slit have aspect ratios of around 7, equating approximately to two-dimensional flow (Wales 1976), the inlet and outlet to the contraction–expansion have an aspect ratio of order 1, and thus three-dimensional flow is expected in this region. Because of the enclosed nature of the system, there was no noticeable degradation of the material during the processing experiment.

Stress-induced birefringence was captured using monochromatic polarised light with a wavelength of 514 nm, which passed through the midsection and orthogonal analyser before being captured using a digital video camera. Quarter wave plates were used to eliminate the isoclinic extinction bands and leave only the stress-related isochromatic fringes. For the bright field visualization of flow induced crystallization, these optics were removed.

The flow through the two geometries was characterised in the following way: The apparent wall shear rate used to characterise flow through the CE slit was based on the solution for Newtonian flow through infinite parallel plates and is given by,

$$\dot{\gamma}_{app} = \frac{6Q}{w^2 l} = \frac{150\pi V_p}{w^2 l} \quad (1)$$

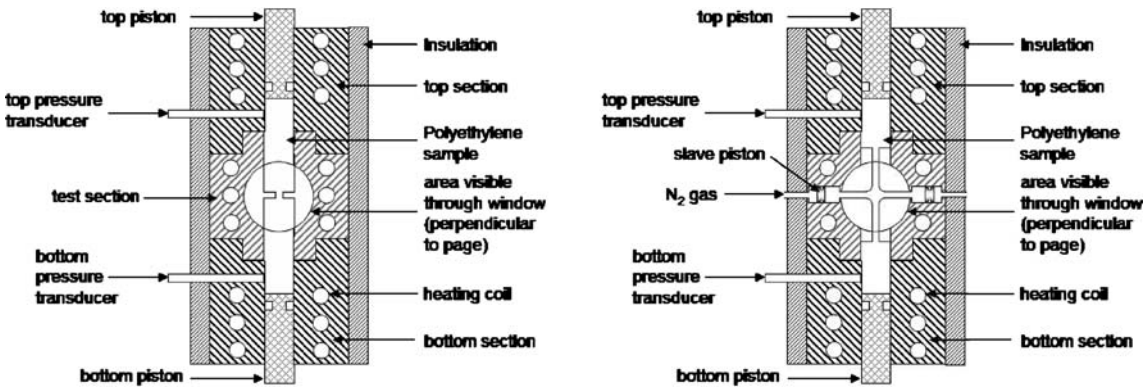

Fig. 2 Schematic outlining the MPR design of (*left*) the contraction–expansion slit and (*right*) the cross-slot

where Q is the volumetric flowrate (mm^3 s^{-1}), w is the width of the slit (1.4 mm), l is the depth of the slit (10 mm) and V_p is the speed of the pistons (mm s^{-1}).

The central extension rate in the cross-slot was estimated from the flow geometry, and the relationship between the maximum extension rate and the piston speed was defined as

$$\dot{\varepsilon}_{\max} = AV_p \tag{2}$$

where A is a constant defined by the geometry. As an approximation, the centre line velocity accelerates from zero at the centre to the maximum channel velocity within the cross-slot over a distance equal to the channel width. Numerical simulations using a Newtonian and integral Wagner model were initially performed by Coventry (2006) and found A to be equal to approximately 8. Subsequent modelling using the multi-mode POM-POM constitutive model for various lightly branched polyethylenes found A equal to 8.6, and this value was used in the subsequent sections.

Results and discussion

Birefringence

Figure 3 shows the steady flow principal stress difference (PSD) for flow through the two geometries at 155 °C. The apparent wall shear rate for the contraction–expansion slit flow was ~24 s^{-1}, and for the cross-slot flow, central extension rate was ~3.8 s^{-1} with a wall shear rate of ~9.2 s^{-1}. The fringe numbers, f, highlighted in the figure, correspond to increasing levels of PSD as defined by the stress-optical rule (see for instance Macosko 1994). As stated previously, both flows exhibit regions of simple shear close to the walls and extensional flow along the symmetry planes of the flow. This is in the central entry and exit region of the CE slit and along the outlet centre line near the stagnation point for the cross-slot. The stress pattern in the CE slit shows asymmetry between the slit inlet and outlet and the formation of stress fangs, similar to those reported in previous work (Lee et al. 2001). The greatest level of stress, counting back from the zero stress "eye" at the slit outlet where the polymer has relaxed subsequent to entry into the slit, shown as f=0 in the figure, is clearly seen to be at the walls of the slit. This is not unexpected as it is within this region that the simple shear is greatest. For the cross-slot, an asymmetric fringe pattern between the inlet and outlet is seen, similar to previous observations (Verbeeten 2001; Soulages et al. 2007 and Coventry and Mackley 2008), with an additional formation of a "W" cusp fringe pattern at the outlet centre line. The formation of this

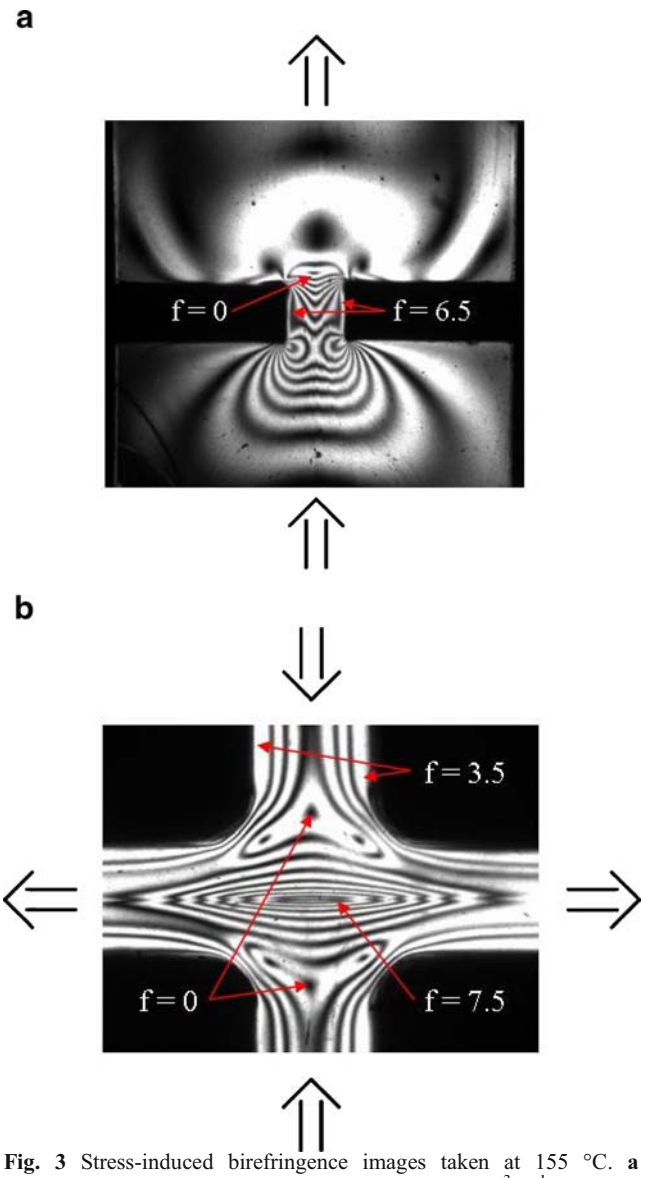

Fig. 3 Stress-induced birefringence images taken at 155 °C. **a** Contraction-expansion, volumetric flow rate 78.5 mm^3 s^{-1}, apparent wall shear rate within the slit ~24 s^{-1}. **b** Cross-slot, volumetric flow rate through each channel 34.5 mm^3 s^{-1}, wall shear rate ~9.2 s^{-1}, maximum extension rate ~3.8 s^{-1}

W cusp has been observed for other highly branched materials using both this cross-slot device (Hassell et al. 2008) and elsewhere (Soulages et al. 2007), and this will be discussed in more detail in subsequent work. It is thought to be the result of extreme strain hardening at the centre line, and the appearance of this local singularity may be related to "birefringent pipes" reported for exit flow in certain polymer solutions (Harlen et al. 1990, 1992). For the cross-slot flow, the PSD in the regions of high extension near the centre line is much higher than for similar levels of simple shear near the wall and is believed to be the result of the increased orientation and chain stretch within this type of flow. In both flows, the high levels of PSD are at areas of

high molecular orientation, either at the slit wall because of shear or at the cross-slot outlet centre line due of extension.

Bright-field crystallisation observations

After the birefringence measurement experiments had been carried out, the material was cooled to 125 °C over a period of 20–30 min, allowing the previous flow history to return to their quiescent state. The flow was then repeated for both geometries at the same flow conditions used for the PSD measurements, and FIC was visualised using bright-field techniques. Flow rate and temperatures were chosen, which gave the best optical clarity and kinetics for observation. One complete multi-pass cycle was performed for the two geometries, which for the CE slit involved two runs at the same flowrate. For the cross-slot, the rate of return flow was reduced to 3.45 $mm^3\ s^{-1}$ per inlet to avoid entrainment of N_2 gas past the slave pistons and into the polymer. The molecular relaxation time-scales at the crystallisation temperature will be longer than those at the higher temperature birefringence experiments. While this will correspond to an increase in the effective flow Weissenberg number, this does not effect the location of the regions of high stress within the flows. The Weissenberg number has been used with success in previous studies to illustrate the dependence of relaxation times on shear-induced crystallisation for various branched polyethylenes (Bustos et al. 2006). In this study, the relaxation spectrum could only be acquired at 155 °C between $0.01<\lambda<100$ s, which did not

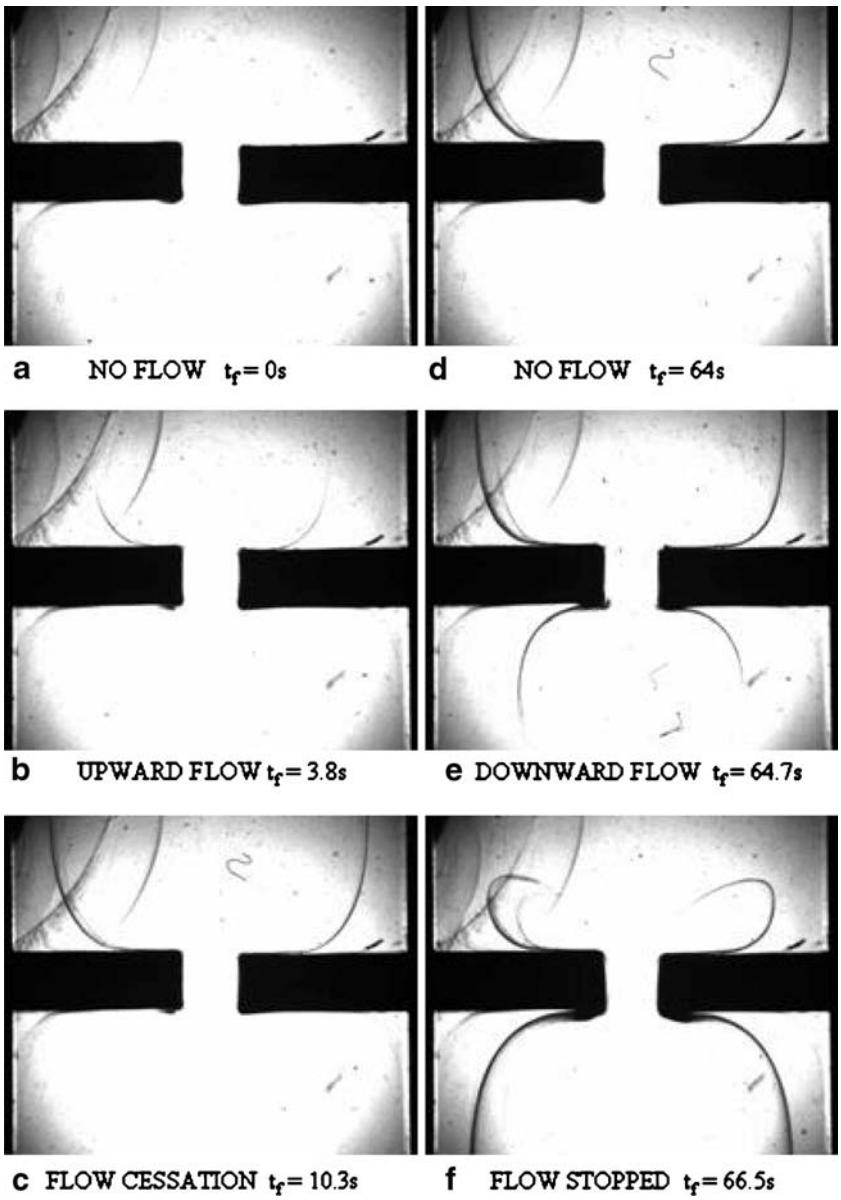

Fig. 4 Bright-field crystallisation during flow within the contraction–expansion geometry at 125 °C, apparent wall shear rate within the slit ~24 s^{-1}. t_f represents the time after the beginning of flow. t_r represents the time after the beginning of flow in the reverse direction. **a** t_f=0 s, no crystallisation present. **b** t_f=3.8 s, crystals have formed at the high-strain region at the slit wall and outlet corners and begin to travel downstream with the flow. **c** t_f=10.3 s, cessation of flow. **d** t_f=64 s, over 50 s after flow has stopped and no visible change in the crystalline material is observed. **e** t_f=64.7 s, t_r=0.7 s, on flow reversal, a similar process of crystal formation and migration downstream from the high-strain regions is observed but occurs more quickly than in the first pass. **f** t_f=66.5 s, t_r=2.5 s, the upstream crystal filament travels back towards the slit with the flow, while downstream of the slit the crystal filament is propagated in a similar manner as in the earlier pass

fully capture the broad relaxation spectrum and the contribution of the high molecular weight (M_w) tail. The average relaxation time based on this spectrum, used to define the Weissenberg number within the two flows, will not be a true representation of the material and molecular stretch. As a result, this approach is not used in the following discussion, although direct comparison of shear and extensional rates is valid as the material and temperatures are constant for both geometries. Because of the complex nature of the streamlines present within the two devices, it was also impractical to calculate the specific work of deformation on the materials as carried out by Janeschitz-Kriegl et al. (2003).

Figure 4 shows the development of crystallisation over time for the CE slit flow, and Fig. 5 illustrates the matching development seen in Fig. 4 once the background zero flow image is removed. The observed flow birefringence pattern within the slit geometry was consistent with previous studies (Hernandez de Muller 2007), where crystallisation occurred at the slit wall outlet corner before being advected downstream from the slit. Subsequent growth occurred as a downstream filament emanating from the downstream lip of the slit, which is clearly seen in Fig. 5, and the crystal filament forms a fang pattern similar to the stress birefringence pattern. Reversal of the flow, seen in Fig. 4e, f, illustrates the stability of the initial FIC and the repeatability of the process. The crystallisation on flow reversal occurs more quickly than on the first pass because of the previous orientation and nucleation of the proceeding flow. In particular, the results show that for this polymer in

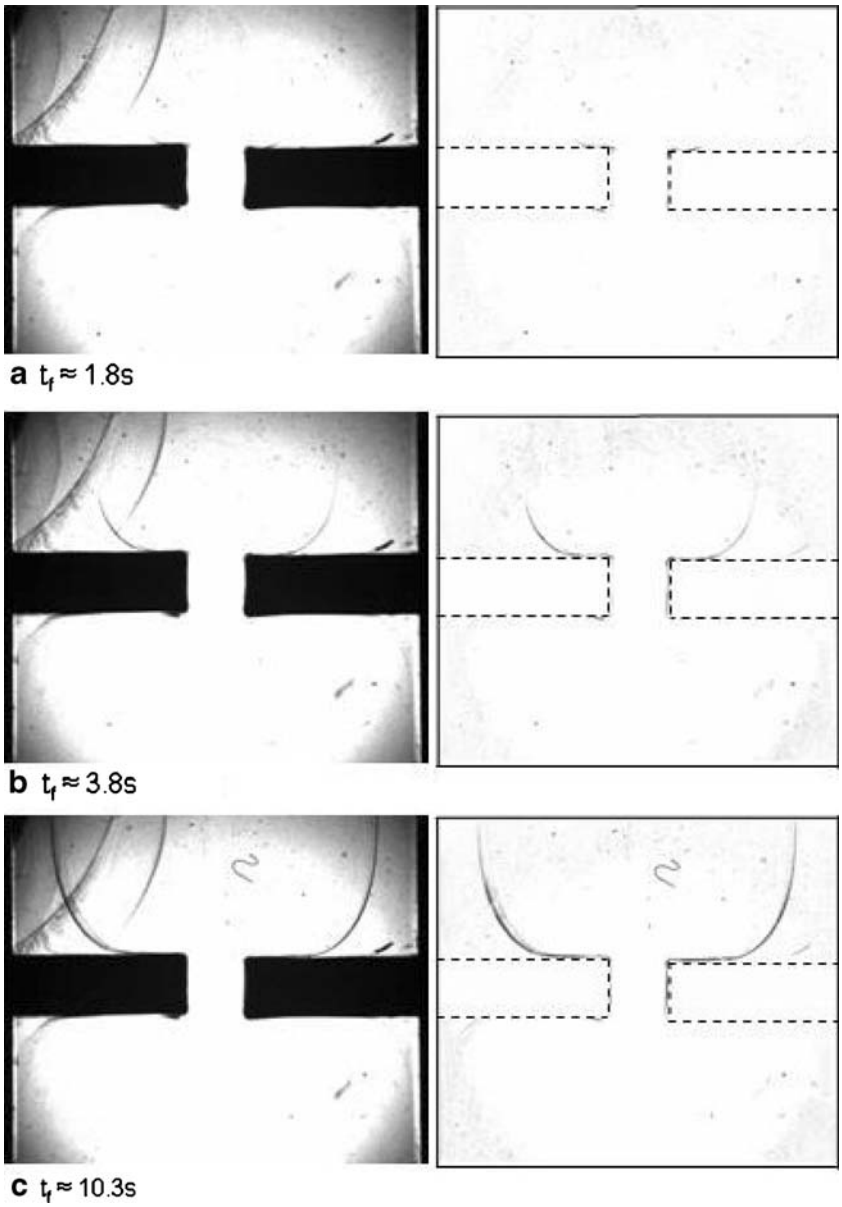

Fig. 5 Crystal development within the slit geometry. (*Left*) The raw image and (*right*) the image after the raw image at t_f=0 has been removed for (**a**–**c**) times t_f=1.77, 3.8 and 10.3 s, respectively. The development of the filament strand occurs initially at the corner of the slit outlet before propagating downstream with the flow

this particular geometry at the temperature under test, FIC occurs initially at the wall and edges of the slit. In this region, the flow is dominantly simple shear. For these flow conditions, FIC was not observed in either the upstream or downstream centre line extensional region of the flow. These observations are similar to those reported for polyethylene solutions (Pennings 1977), which proposed a growth mechanism of bundle-like nucleation caused by stretching of an entanglement network attached to the surface.

Advection of the crystal filament tip downstream was tracked with time and is presented in Fig. 6 for both flow passes. As expected from viewing Fig. 4, the left and right crystal trajectories are symmetric for each pass. Slight discrepancies are observed and are the result of the difficulty involved with accurately capturing the precise filament tip location for each time. The trajectory of the crystal fibre tip is observed to be different between pass one and two. This is probably due to the increased kinetics of the already pre-aligned material within the slit resulting in increased fibre growth during the second pass, obvious from the increased growth observed in Fig. 4. This would then result in a modified flow profile because of the increased constriction in the slit caused by crystal growth at the walls.

Figure 7a illustrates the left and right hand filament tip progression for the first pass alongside that observed for three particles seen within the flow over the course of the experiment. The flow field is transient with time, shown by the cross-over of the trajectories of the right crystal filament tip and that of P3. P3 does not cross the crystal filament but instead moves along a streamline close to the crystal (see Fig. 8 for a comparison of crystal and particle). Over time, the crystal filament moves further along the slit wall before detaching into the molten polymer. This results in a net

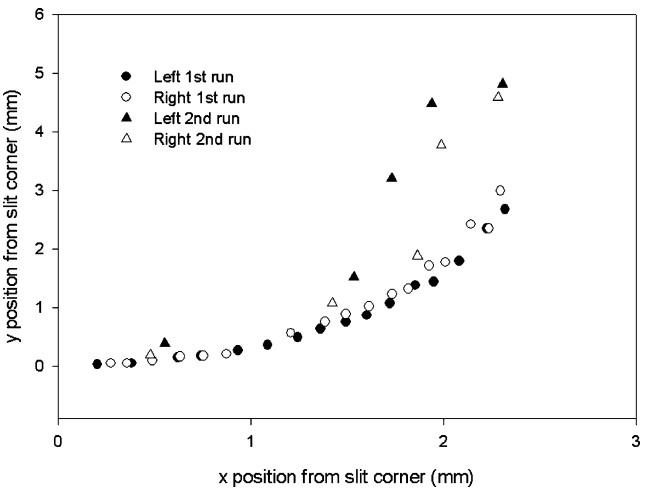

Fig. 6 Graph illustrating the crystal tip position with respect to the slit corner at various times for the left (*filled*) and right (*open*) crystal filaments for the two passes

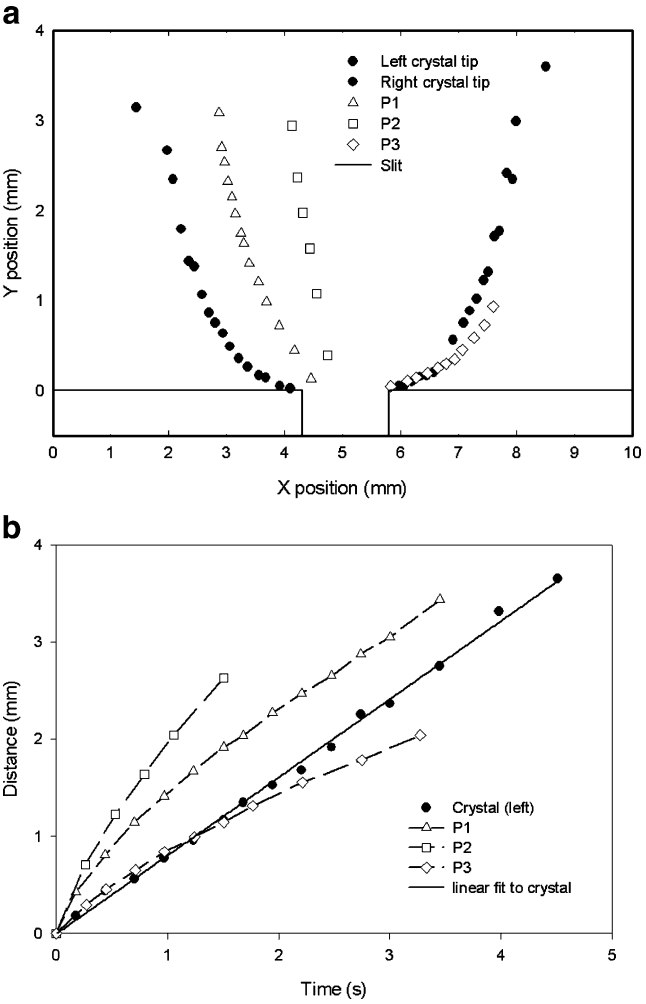

Fig. 7 **a** Graph showing the position of particles (*open*) and the crystal filament tip (filled) within the flow at various times for pass one, illustrating their trajectory. **b** The corresponding graph of distance travelled as a function of time for the particles and crystal tip. The right crystal filament was found to follow the same linear fit as the left but with more noise and has not been included for clarity. The distance at time t is defined as the summed distances at all previous times, $D_{t+1}=D_t+\Delta D$

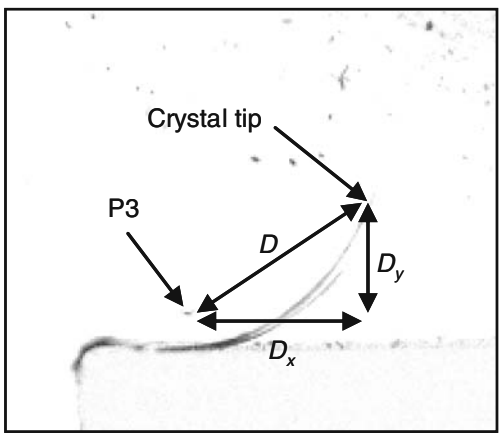

Fig. 8 Graph showing position of P3 in relaxation to the crystal tip. The distance between P3 and the tip is defined as D, while the distances in the x and y axes are given as D_x and D_y, respectively

movement of the advected material further from the slit in the direction perpendicular to the bulk flow. Assuming that the particles follow the fluid and do not modify the flow itself, a graph illustrating the distance the particles move as a function of time from when they first move away from the slit outlet is given in Fig. 7b. The velocities of the individual particles, represented as the gradient of the curve, are seen to decrease as they move away from the slit. This is unsurprising, as the material is flowing into an expansion and is thus expected to slow down. The velocity of the crystal tip, however, is seen to remain constant with time. This illustrates that the crystal filament does not slow down as it leaves the contraction and moves more quickly away from the slit than the surrounding fluid. This is best shown by the comparison of the tip velocity and that of P3, the particle observed closest to the filament during the course of its development. It is seen that while P3 initially has a velocity greater than the filament tip, over time it slows until its velocity is less than the filament tip.

To further illustrate this, Figs. 8 and 9 show the distance between the filament tip and P3 as a function of time. The distance between the two, D, was plotted alongside the distance in the bulk flow direction (D_y) and that perpendicular to the bulk flow (D_x). These distances are shown in Fig. 8. If both travel along their respective streamlines and follow the flow field, then over time P3 should catch up slightly to the filament tip assuming that no further crystal growth occurs at the tip. D_x, would become smaller as the particle moved along its streamline, away from the slit exit and towards the developed channel flow downstream. At the same time, D_y would initially increase as the main flow of the tip is in this direction, but over time, this would stabilise as the trajectory of P3 followed the bulk flow direction. In reality, the distance between P3 and the tip

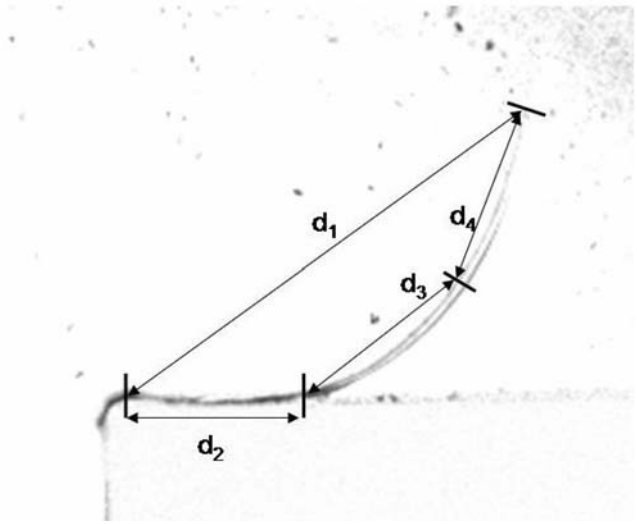

Fig. 10 Approximation of fibre contour length, $L_1=d_1$, $L_2=d_2+d_3+d_4$

increases with time, and while as expected, D_x decreases with time, the increase in distance D is result of a continually increasing distance in the bulk flow direction, D_y. This indicates that the filament is accelerating away from the bulk flow in the downstream direction and that the downstream filament velocity is defined by conditions within the slit rather than local flow conditions.

The length of the crystal filaments can be determined using a range of techniques, and various filament segment distances are highlighted in Fig. 10. As stated previously, the filament begins at the slit and moves along the slit wall until a certain point before detaching. It then curves downstream in an arch, similar to stress birefringent fangs observed in previous work (Lee et al. 2001). Two techniques are plotted in Fig. 11 as a function of filament

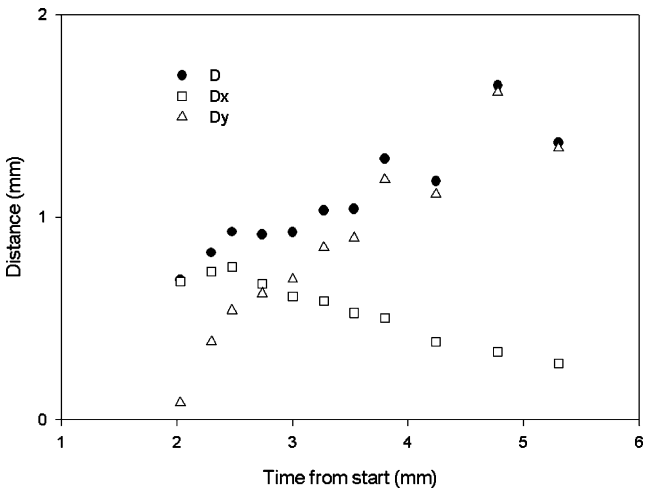

Fig. 9 Graph of D, D_x and D_y as defined in Fig. 8 against time from start of flow

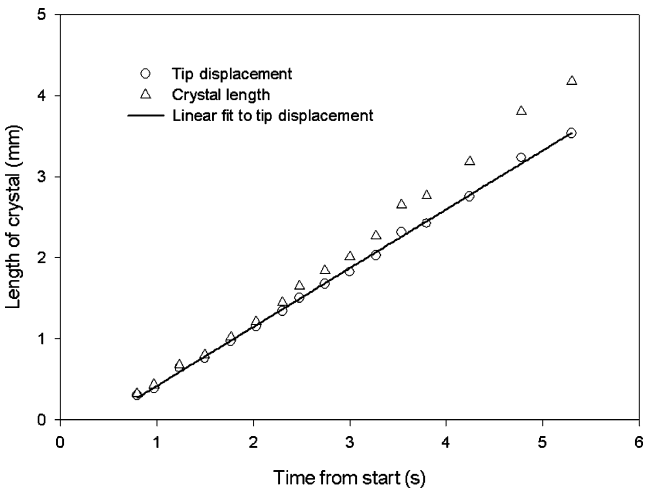

Fig. 11 Graph of crystal length (L_2) and tip displacement (L_1) against time from the start of flow

length against time for the case of the left hand filament. The first technique uses the distance from the filament tip to the slit corner as a crude indication of the length, where $L_1=d_1$. The second uses a more accurate approach and takes into account the length of filament at the wall and a simple approximation of the curved length, where $L_2=d_2+d_3+d_4$.

While the crude approximation of filament length, L_1, is a linear function of time, indicating a constant formation of crystal within the filament, the gradient of the more accurate definition of crystal length, L_2, is seen to increase with time. This indicates that the rate of growth of the crystal filament increases over time. The results in Figs. 7b and 9 indicate that the tip moves relative to the surrounding fluid, and previous work showed that this led to crystal growth at the tip (Mackley 1975). However, the movement of the tip relative to the surrounding flow is opposite in this case, and it is unclear how this flow could lead to an increase in growth at the tip. It is more likely to be a result of the conditions within the slit itself. Equally, it is possible that the crystal growth within the slit leads to a modified flow field, resulting in increased shear and FIB. Another possibility is the increased tethering of the filament to the wall resulting in increased growth because of a process similar to that outlined by Pennings (1977). At this stage, it is uncertain what the exact mechanism for the enhanced growth is, although it is clear that the crystal does not flow downstream with the local flow field.

The cross-slot observations shown in Figs. 12 and 13 illustrate the time evolution of FIC. Figure 12 is the direct bright-field observation and Fig. 13 the observations with the starting image removed. At the start of flow, the black images of the cross-slot inserts of Fig. 12a are clearly identified, and the polymer melt is optically transparent. After flow has commenced, a dark line appears along the central exit symmetry plane of the flow shown in Fig. 12b, and this constitutes FIC in a very localised region of flow. In addition, FIC has occurred at the walls of the cross-slot, and this can only be seen without ambiguity in the right hand image in Fig. 13 where the original image has been subtracted from the final one. On flow reversal, Fig. 12d, it can be seen that the initial centre line filament is advected back along the new exit channel of the cross-slot, demonstrating that the centre line flow-induced crystal is a solid entity. The observation for this geometry shows

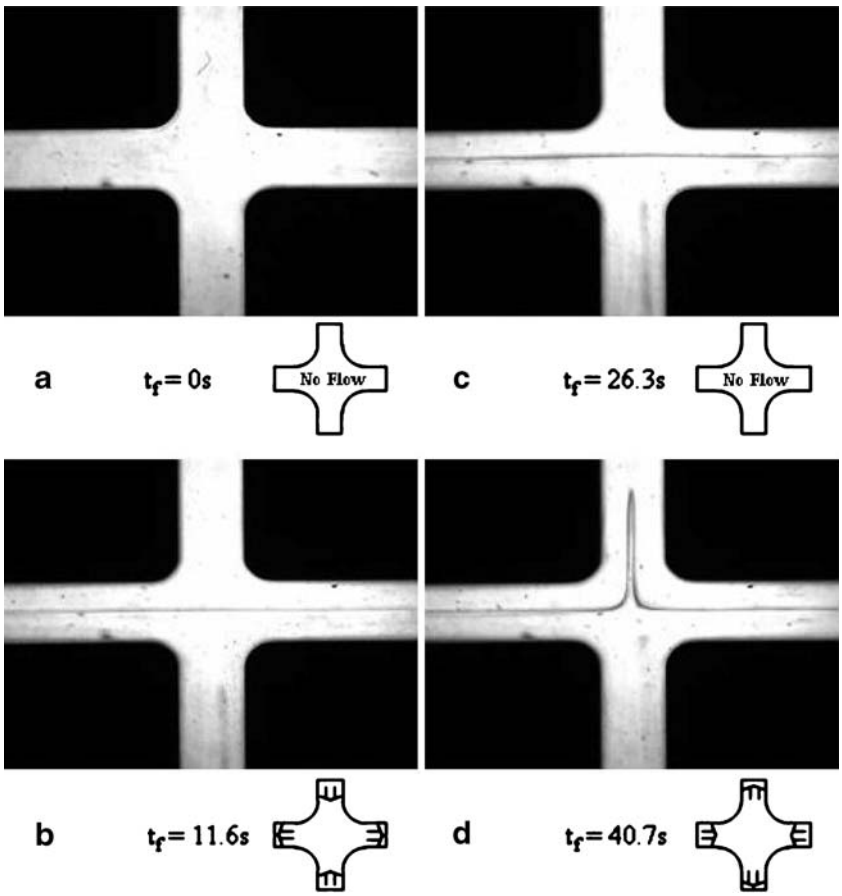

Fig. 12 Bright-field crystallisation during flow within the cross-slot geometry at 125 °C, wall shear rate ~9.2 s^{-1}, maximum extension rate ~3.8 s^{-1}. t_f represents the time after the beginning of flow. t_r represents the time after the beginning of flow in the reverse direction. **a** t_f=0 s, no crystallisation present. **b** t_f=11.6 s, crystallisation appears on the outlet centre line, where the strain is highest, and crystals travel downstream with the flow on the outlet centre line. **c** t_f=26.3 s, no visible increase in crystallisation is seen ~15 s after cessation of flow. **d** t_f=40.7 s, t_r=14.4 s, flow is reversed and the crystal fibre is transported upstream in one direction with the flow, although no further extensional crystallisation occurs because of the reduced flow rate and associated extension rate and strain. The crystal fibre retains its integrity for the reversal of flow

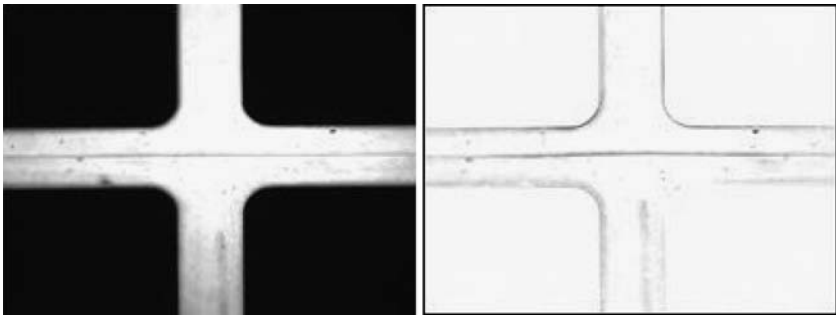

Fig. 13 Crystal development within the cross-slot geometry after the cessation of flow (t_f= 11.6 s) for the first pass. (*Left*) raw image and (*right*) the same image once the t_f=0 image has been removed. This illustrates more clearly not just the formation of crystal filament at the cross-slot centre line but also at the walls because of shear

clearly that nucleation and growth has occurred at the metal walls of the cross-slot and also in the central region of the flow where there are no solid boundary conditions. The centre line observations bear strong similarities to earlier optical observations (Mackley 1972; Crowley et al. 1976) for polyethylene solutions within an impinging jet apparatus and is similar to previous FIC visualisation in a cross-slot device (Swartjes 2001). In these studies, centre line localisation was identified with regions of both pure extensional flow and also high levels of strain (Crowley et al. 1976). Chain extension occurred when the coil stretch transition ($\dot{\varepsilon}\lambda > 1$) occurred, where $\dot{\varepsilon}$ is the extension rate and λ the longest relaxation time of the chain. In addition, $\dot{\varepsilon}t \gg 1$ was necessary to provide sufficient strain to stretch the chain. The strain imposed in the central region is essentially inversely dependant on the distance from the exit symmetry plane (Crowley et al. 1976), and localised fibrous crystallisation is observed here for regions where the level of strain exceeds a certain value. Unfortunately it was not possible to quantify the crystal growth, as for the CE slit flow, as the crystal tip is advected downstream too quickly and no noticeable increase in filament width with time was detected.

These findings demonstrate the sensitivity of FIC to both flow type and the presence of a physical wall. The situation near the wall is dominantly simple shear, where high chain extension may not necessarily be expected, however, it has been previously identified (Pennings 1977; Brochard and deGennes 1992) that the potential for chain stretch of tethered chains to a wall is greater than untethered chains. The results presented here lend support to this concept of enhanced chain extension because of tethered chains.

For both flow geometries, the FIC experiments were carried out at a temperature where quiescent crystallisation would not occur within the time scale of the experiment. At 125 °C, localised FIC occurred for both geometries and if the level of supercooling was increased, i.e. the crystallisation temperature reduced below 125 °C, more massive FIC would occur. The optical observation in the CE slit would then follow observations similar to those of Mackley et al. (1975) and more recently Scelsi (private communication), where massive upstream fibrous crystallisation was observed.

For the situations reported in this paper, FIC nucleates either from the wall or the central region of the cross-slot. The presence of the crystal fibres does not appear to significantly modify the overall flow pattern; however, once formed, the local flow around the fibre will influence the subsequent crystal growth (see for example Mackley et al. 1975).

Conclusions

Results reported in this paper for a well-characterised polyethylene show clearly that highly localised FIC can occur for a particular flow condition, illustrating important features in relation to crystal nucleation and growth. In particular, for the CE geometry, the FIC occurred solely near the walls of the geometry. In this geometry, regions of stretching extensional flow do exist in the upstream region, but the levels of extensional strain in these regions are low when compared to the levels of strain that can be obtained in the cross-slot geometry. The filament was found to advect downstream at velocities greater than the surrounding fluid, and over time, an increase in the kinetics of crystal formation were observed. It is unclear at this point if both phenomena are the result of conditions within the slit. In the case of the cross-slot, FIC was seen both at the walls and also in the central region. The deformation rate in the central region was lower than that at the walls, suggesting that high-strain pure extension is more efficient at nucleating FIC than simple shear flow. The observation also shows that a solid boundary is not an essential component to nucleate FIC for these conditions. Overall, the experimental observations offer scope for comparison with numerical simulation once a suitable model of FIC is developed.

Acknowledgements We would like to acknowledge G. Hernandez de Muller, L. Scelsi, R. Graham and S. Butler for useful help and advice. We also acknowledge the EPSRC for funding through the Microscale Polymer Processing 2 (MUPP^2) program.

References

Acierno S, Palomba B, Henning Winter H, Grizzuti N (2003) Effect of molecular weight on the flow-induced crystallization of isotactic poly(1-butene). Rheol Acta 42(3):243–250

Agassant JF, Baaijens F, Bastian H, Bernnat A, Bogaerds ACB, Coupez T, Debbaut B, Gavrus AL, Goublomme A, van Gurp M, Koopmans RJ, Laun HM, Lee K, Nouatin OH, Makley MR, Peters GWM, Rekers G, Verbeeten WHM, Vergnes B, Wagmer MH, Wassner E, Zoetelief WF (2002) The matching of experimental polymer processing flows to viscoelastic numerical simulation. Int Polym Process XVII 1:3–10

Avrami M (1939) Kinetics of phase change. J Chem Phys 7:1103–1112

Bent J, Hutchings LR, Richards RW, Gough T, Spares R, Coates PD, Grillo I, Harlen OG, Read DJ, Graham RS, Likhtman AE, Groves DJ, Nicholson TM, McLeish TCB (2003) Neutron-mapping polymer flow: scattering, flow visualisation and molecular theory. Science 301:1691–1695

Brochard F, deGennes PG (1992) Shear-dependant slippage at a polymer/solid interface. Langmuir 8(12):3033–3037

Bustos F, Cassagnau P, Fulchiron R (2006) Effect of molecular architecture on quiescent and shear-induced crystallization of polyethylene. J Polym Sci, Part B Polym Phys 44:1597–1607

Byelov D, Panine P, de Jeu WH (2007) Shear-induced smectic order in osotactic polypropylene revisited. Macromolecules 40(2):288–289

Chen Q, Fan Y, Zheng Q (2006) Rheological scaling and modeling of shear-enhanced crystallization rate of polypropylene. Rheol Acta 46:305–316

Coccorullo I, Pantani R, Titomanlio G (2003) Crystallisation kinetics and solidified structure in iPP under high cooling rates. Polymer 44(1):307–318

Collis MW, Mackley MR (2005) The melt processing of monodisperse and polydisperse polystyrene melts within a slit entry and exit flow. J Non-Newtonian Fluid Mech 128(1):29–41

Coventry KD (2006) Cross-slot rheology of polymers. PhD Thesis. University of Cambridge

Coventry KD, Mackley MR (2008) Cross-slot extensional flow of polymer melts using a multi-pass rheometer. J Rheol (in press)

Crowley DG, Frank FC, Mackley MR, Stephenson RG (1976) Localized flow birefringence of polyethylene oxide solutions in a four roll mill. J Polym Sci 14(6):1111–1119

Das C, Inkson NJ, Read DJ, Kelmanson K (2006) Computational linear rheology of general branch-on-branch polymers. J Rheol 50(2):207–234

Doufas AK, Dairanieh IS, McHugh AJ (1999) A continuum model for flow-induced crystallization of polymer melts. J Rheol 43(1):85–109

Guo X, Isayev AI, Guo L (1999) Crystallinity and microsctructure in injection moldings of isotactic polypropylenes. Part 1: a new approach to modelling and model parameters. Polym Eng Sci 39 (10):2096–2114

Haas T, Maxwell B (1969) Effects of shear stress on the crystallisation of linear polyethylene and polybutene-1. Polym Eng Sci 9:225

Hadinata C, Gabriel C, Ruellmann M, Kao N, Laun HM (2006) Shear-induced crystallisation of PB-1 up to processing-relevant shear rates. Rheol Acta 45:539–546

Hadinata C, Boos D, Gabriel C, Wassner E, Ruellman M, Kao N, Laun HM (2007) Elongation-induced crystallisation of a high molecular weight isotactic polybutene-1 melt compared to shear-induced crystallisation. J Rheol 51(2):195–215

Harlen OG, Rallison JM, Chilcott MD (1990) High-Deborah-number flows of dilute polymer solutions. J Non-Newtonian Fluid Mech 34:319–349

Harlen OG, Hinch EJ, Rallison JM (1992) Birefringent pipes: the steady flow of a dilute polymer solution near a stagnation point. J Non-Newtonian Fluid Mech 44:229–265

Hassell DG, Auhl D, McLeish TCB, Mackley MR (2008) The effect of viscoelasticity on stress fields within polyethylene melt flow for a cross-slot and contraction-expansion slit geometry. Rheol Acta DOI 10.1007/s00397-008-0261-8

Heeley EL, Fernyhough CM, Graham RS, Olmsted PD, Inkson NJ, Embery J, Groves DJ, McLeish TCB, Morgovan AC, Meneau F, Bras W, Ryan AJ (2006) Shear-Induced crystallization in blends of model linear and long chain branched hydrogenated polybutadienes. Macromolecules 39(15):5058–5071

Hernandez de Muller G (2007) The effect of flow on the crystallisation of polyethylene. PhD Thesis. University of Cambridge

Iguchi M, Matsumoto T, Tonami H, Kawai T, Maeda H, Mitsusuhashi S (1966) Solution grown polymer crystals. Int Symp Macromulecular Chemistry 4.5:12

Janeschitz-Kriegl H (2003) How to understand nucleation in crystallizing polymer melts under real processing conditions. Colloid Polym Sci 281:1157–1171

Janeschitz-Kriegl H, Ratajski E, Stadlbauer M (2003) Flow as an effective promoter of nucleation in polymer melts: a quantitative evaluation. Rheol Acta 42:355–364

Jay F, Haudin JM, Monasse B (1999) Shear-induced crystallisation of polypropylenes: effect of molecular weight. J Mater Sci 34:2089–2102

Keller A (1968) Polymer crystals. Rep Prog Phys 31:623–704

Kimata S, Sakurai T, Nozue Y, Kasahara T, Yamaguchi N, Karino T, Shibayama M, Kornfield JA (2007) Molecular basis of the shish-kebab morphology in polymer crystallization. Science 316:1014–1017

Lee K, Mackley MR, Mcleish TCB, Nicholson TM, Harlen O (2001) Experimental observation and numerical simulation of transient stress fangs within flowing molten polyethylene. J Rheol 45 (6):1261–1277

Mackley MR (1972) Flow induced polymer chain extension and its relationship to fibrous crystallization. PhD Thesis, University of Bristol

Mackley MR (1975) Shish kebabs: hydrodynamic factors affecting their crystal growth. Colloid Polym Sci 253:373

Mackley MR, Frank F, Keller A (1975) Flow induced crystallisation of polyethylene melts. J Mater Sci 10:1501–1509

Mackley MR, Marshall RTJ, Smeulders JBAF (1995) The multipass rheometer. J Rheol 39(6):1293–1309

Mackley MR, Moggridge GD, Saquet O (2000) Direct experimental evidence for flow induced fibrous polymer crystallisation occurring at a solid/melt interface. J Mater Sci 35:5247–5253

Macosko CW (1994) Rheology, principles, measurements and applications. Wiley, New York

Nogales A, Hsiao BS, Somani RH, Srinivas S, Tsou AH, Balta-Calleja FJ, Ezquerra TA (2001) Shear-induced crystallization of isotactic polypropylene with different molecular weight distributions: in situ small- and wide-angle X-ray scattering studies. Polymer 42 (12):5247–5256

Pennings AJ (1977) Bundle-like nucleation and longitudinal growth of fibrillar polymer crystals from flowing solutions. J Polym Sci, Polym Symp 59:55–86

Pennings AJ, Kiel AM (1965) Kolloid Z Z Polym 1965 205:160

Peters GWM, Schoonen JFM, Baaijens FPT, Meijer HEH (1999) On the performance of enhanced constitutive models for polymer melts in a cross-slot flow. J Non-Newtonian Fluid Mech 82:387–427

Smirnova J, Silva L, Monasse B, Chenot J, Haudin J (2005) Structure development in injection molding. Int Polym Process 20(2):178–185

Soulages J, Schweizer T, Venerus DC, Hostettler J, Mettler F, Kroger M, Ottinger HC (2007) Lubricated optical rheometer for the study of two-dimensional complex flows of polymer melts. J Non-Newtonian Fluid Mech. DOI 10.1016/j.jnnfm.2007.10.006

Swartjes FHM (2001) Stress induced crystallisation in elongational flow, Ph.D. Thesis. Eindhoven Univeristy of Technology, downloadable from: http://www.mate.tue.nl

Valette R, Mackley MR, Hernandez Fernandez del Castillo G (2006) Matching time dependent pressure driven flows with a Rolie Poly numerical simulation. J Non-Newtonian Fluid Mech 136(2–3): 118–125

van der Vegt AK, Smit PPA (1967) Crystallization phenomena in flowing polymers. Adv Polym Sci 26:313

van Meerveld J, Peters GWM, Hutter M (2004) Towards a rheological classification of flow induced crystallisation experiments of polymer melts. Rheol Acta 44:119–134

Verbeeten WMH (2001) Computational polymer melt rheology. PhD Thesis. Eindhoven Univeristy of Technology, downloadable from http://www.mate.tue.nl

Wales JLS (1976) The application of flow birefringence to rheological studies of polymer melts. PhD Thesis, Delft University of Technology, Delft

Wood-Adams P, Costeux S (2001) Thermorheological behaviour of polyethylene: effects of microstructure and long chain branching. Macromolecules 34:6281–6290

Zuidema H, Peters GWM, Meijer HEH (2001) Development and validation of a recoverable strain-based model for flow-induced crystallization of polymers. Macromol Theory Simul 10:447–460